Simulation of 3-Staged MPC Using Custom Characteristics of Magnetic Cores

Jaegu Choi, Takao Namihira, Takashi Sakugawa, Sunao Katsuki and Hidenori Akiyama

Kumamoto University.
Kurokami 2-39-1
Kumamoto, Kumamoto 860-8555, Japan

ABSTRACT

A low inductance circuit has been fabricated in order to obtain shorter time to saturation during core unsaturation and current pulses with shorter widths during core saturation. B-H curves have been derived from the measured voltage and current waveforms. Characteristics of the magnetic core for pulsed-power generators have been investigated and the Electromagnetic Transient Program (EMTP) simulation has been carried out in order to determine the effects of leakage current on the energy efficiency of a 3-staged magnetic pulse compressor (MPC). As results, the derived B-H curves show the following characteristics: a high ratio of unsaturated to saturated permeability (μ_{un}/μ_{sat}), a maximum flux swing of about 2.55 T, a high ratio of remanent flux density to saturation magnetic flux density (B_r/B_s) and low core loss. And, it is found that μ_{un} increases with time to saturation and that μ_{sat} is strongly influenced by the stray inductances of the core. By applying custom characteristics to each stage in EMTP simulation, more practical energy transfer in MPC is obtained.

Index Terms — *B-H* curve, leakage current, magnetic core, MPC, EMTP.

1 INTRODUCTION

RECENT developments in ferromagnetic materials [1], [2] and semiconductor switches have allowed high repetitive operation of magnetic switches (MS) [3-7] with very low losses, and have made it possible to use repetitive pulsed power generated by magnetic pulse compressors (MPC) in practical industrial applications such as laser exciters, decomposition of hazardous gases, removal of volatile toxic compounds and water treatment [8-15]. The magnetic switch used in pulsed-power applications is superior in its high repetition rate, high stability, and long lifetime to electrical discharge switches that have unstable switching and short lifetimes due to electrode deterioration. The saturable inductor (SI) works as a switch by blocking current with a high inductance during the unsaturated state and passing current with a low inductance during the saturated state. Eligible magnetic materials for repetitive pulsed-power applications must have the following characteristics: a high ratio of unsaturated to saturated permeability (μ_{un}/μ_{sat}), a high flux swing, a high saturation flux density (B_s) and remnant flux density (B_r), and low core loss.

The dc and ac characteristics of magnetic materials have been well known and easy to obtain from manufacturers. As the use of magnetic cores has become popular in pulsed-power applications, there have been several studies of the pulse magnetic characteristics that are critical for a multi-

stage MPC [16-20]. However, there are still some necessities for the users of the magnetic cores to measure the pulse characteristics for more efficient MPC design. As the number of stages in an MPC increases, the efficiency of the energy transfer that is one of the dominant measures for overall performance becomes poor.

In this paper, a low inductance circuit fabricated to obtain shorter time to saturation during core unsaturation and current pulses with shorter pulse widths during core saturation is described. Also, the characteristics of the magnetic core for pulsed-power applications are described using the *B-H* curves derived from the measured voltage and current waveforms. Finally the Electromagnetic Transient Program (EMTP) simulation is carried out in order to determine the effects of leakage current on the energy efficiency of a typical 3-staged MPC.

2 EXPERIMENTAL SETUP AND PROCEDURES

Figure 1 describes the schematic diagram of the low inductance circuit for measuring dynamic properties of the magnetic core. The discharge circuit has a coaxial geometry to reduce the stray inductance of the circuit. The total inductance around the main current loop during saturation of the core has been calculated to be as low as about 85 nH using equation (3). A reset circuit is used to obtain a maximum flux swing. The magnetic core used in this study is a FINEMET core (FT-1H, Hitachi Metal Corp., Japan),
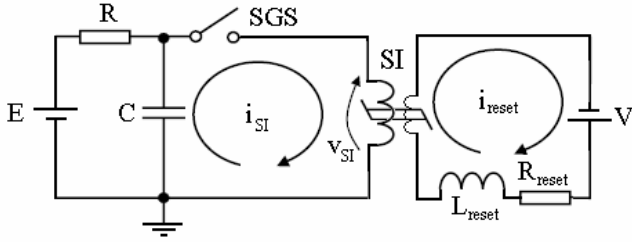
Figure 1. Schematic diagram of the low-inductance circuit for measuring dynamic properties of the magnetic core.
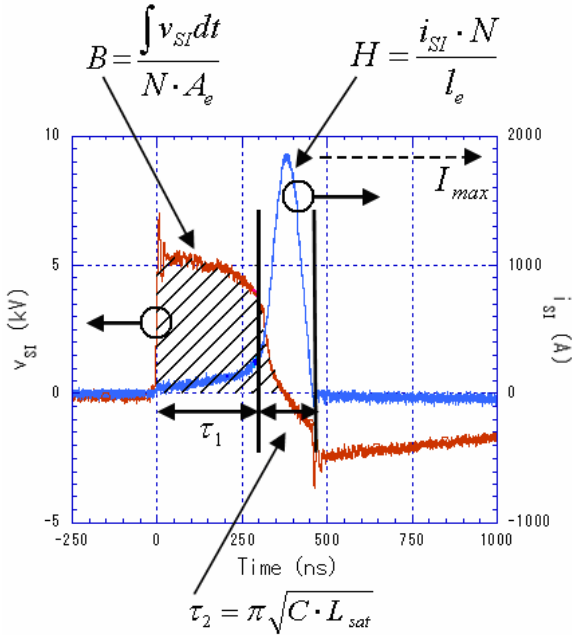

Figure 2. Derivation method for *B-H* curves from the measured voltage and current waveforms.

which has a 60 mm inner diameter, 130 mm outer diameter and is 25.4mm in height.

In Figure 1, a dc voltage source (E) is used to charge a capacitor (C) through a high resistance (R). On closure of the triggered spark gap switch (SGS), the SI begins to saturate after time to saturation, τ_1. The applied voltage across the SI, v_{SI} and the discharge current, i_{SI} have been measured using a voltage divider (EP-50K, Pulse Electronic Engineering Co., Japan) and a current monitor (Model 110A, Pearson Electronics, USA), respectively. An oscilloscope (TDS3054B, 500 MHz, Tektronix) recorded the single-shot signals from the measurement devices.

Figure 2 illustrates the derivation method for the *B-H* curves from the measured voltage and current waveforms. The flux density, *B*, is obtained from [6]:

$$B = \frac{\int v_{SI} dt}{N \cdot A_e} \tag{1}$$

where *N* is the number of winding turns and A_e is the effective cross-section area that is the actual area of the magnetic material in the core excluding the area of the inter-laminar insulation.

Table 1. Experimental parameters.

# of core	C (nF)	E (kV)	τ_1 (ns)	τ_2 (ns)	L_{sat} (nH)	
1	5	20.0	108	65	86	Case 1
	25	9.0	187	145	85	Case 2
	100	4.5	365	395	150	Case 3
2	5	20.0	203	65	86	Case 4
	25	9.0	400	145	85	Case 5
	100	4.5	755	395	150	Case 6

The magnetic field, *H*, is given by:

$$H = \frac{i_{SI} \cdot N}{l_e} \tag{2}$$

where l_e is average magnetic path length.

Time to saturation, τ_1, and current pulse width τ_2 can be used in deriving several physical quantities. However, it is very difficult to exactly determine the boundary line of the two terms in Figure 2 because the current pulse at earlier times is distorted by the saturation of the core. Therefore, τ_1 and τ_2 are determined by the following iterative procedure in this study. First, the current pulse width, τ_2, is roughly determined from the measured current waveform. τ_1 is then calculated from the voltage and current waveforms. In order to verify these values, the circuit inductance at SI saturation L_{sat} is obtained from:

$$L_{sat} = \frac{(\tau_2/\pi)^2}{C} \tag{3}$$

and the voltage at τ_1 is obtained from [17]:

$$v_{\tau_1} = I_{max} \cdot \sqrt{\frac{L_{sat}}{C}} \tag{4}$$

where I_{max} and *C* are the maximum current value and capacitance, respectively. τ_1 can then be determined in accordance with v_{τ_1} from the voltage waveform. Finally, this τ_1 is compared with the roughly determined one. If there is a significant difference between them, a new value of τ_2 is taken. The procedure is repeated until the values are equal to each other. The results are shown in Table I with the experimental parameters. L_{sat} of 100 nF is larger than those of others because of the different geometry of the capacitor. The reset current was chosen as 0.5 A or 1.0 A in order to get a more coercive force than the 0.6 A/m that is recommended by the manufacturer. The frequency of the current pulse during saturation can be determined from:
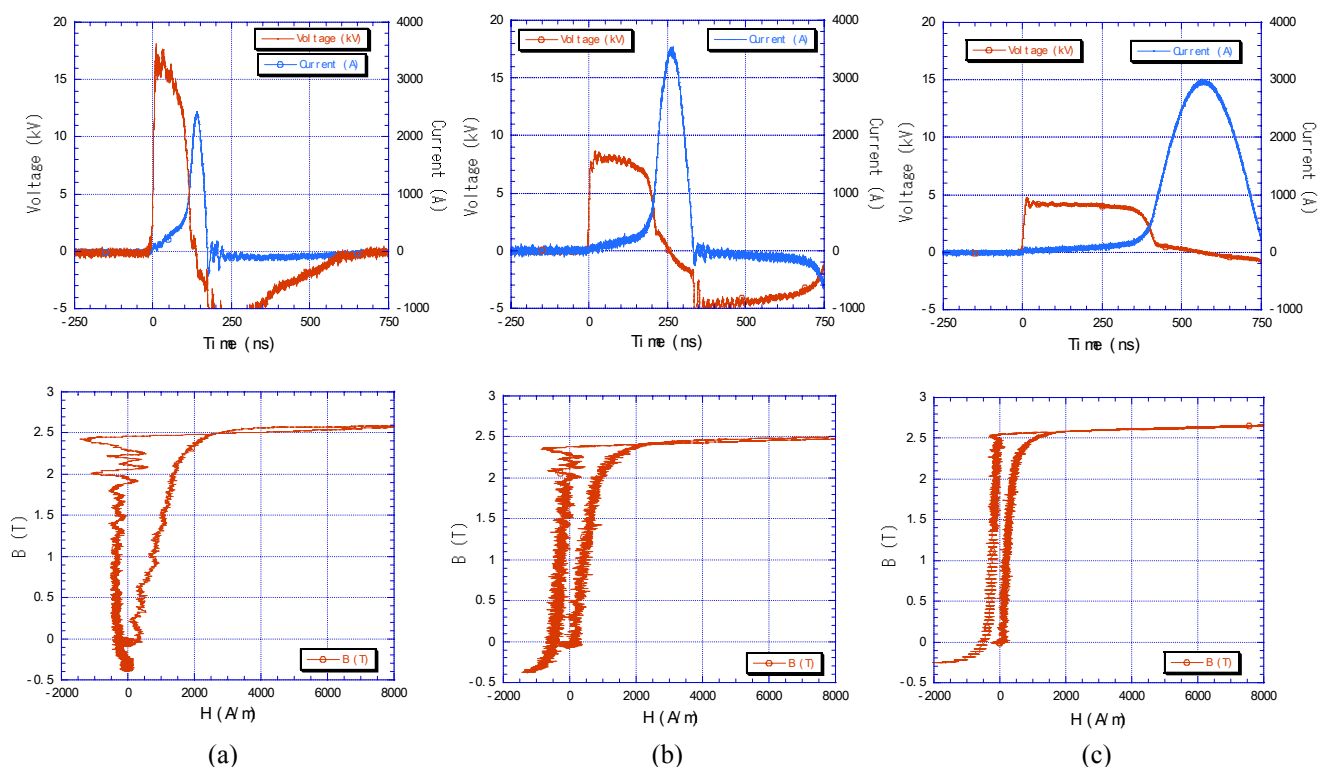
$$f_{sat} = \frac{1}{2\tau_2} \tag{5}$$

Figure 3. Typical voltage and current waveforms (top) and derived *B-H* curves (bottom) in case of 1 core, (a) capacitance of 5 nF and voltage of 20 kV, (b) capacitance of 25 nF and voltage of 9 kV and (c) capacitance of 100 nF and voltage of 4.5 kV.

3 RESULTS AND DISCUSSION

3.1 DERIVATION OF B-H CURVES

Figure 3 shows the typical voltage and current waveforms (top) and derived *B-H* curves (bottom) for the case of one single core and reset current of 1.0 A. In the voltage and current waveforms, on closure of the triggered SGS at 0 ns, most of the charge voltage is applied across the SI. It is observed that the leakage current increases as time increases and that τ_1 increases with decreasing voltage because the product of voltage and time is constant. After τ_1, the SI reaches saturation and operates as a closing magnetic switch. The trend of the maximum current can be explained by equation (4).

The *B-H* curves are derived from the measured voltage and current waveforms using equations (1) and (2). From the hysteresis loops, it can be seen that ① the ratio of unsaturated to saturated permeability (μ_{un}/μ_{sat}) is very large, which means very good switching performance, ② the maximum flux swing over 2.5 T is obtained by applying a reset current greater than a current value corresponding to the coercive force H_c of the magnetic core, which means that this core can contribute to the compact pulsed-power generators, ③ the ratio of remnant flux density to saturation magnetic flux density (B_r/B_s) is close to 1, which means good switching performance and ④ low core loss is

expected from the narrow area of the hysteresis loop, which means that repetitive operation is possible.

Dependence of unsaturated relative permeability (μ_{ru}) on time to saturation (τ_1) is shown in Figure 4. It can be seen that μ_{ru} increases with τ_1 for a fixed product of voltage and time. This is because μ_{ru} increases with decreasing dB/dt, that is, decreasing voltage [16]. From these results, it is considered that the last stage in MPC will show worse switching performance because it has a shorter τ_1 and a larger leakage current. Also, it is observed that the permeability of two cores is higher than that of one core due to the fact that dB/dt has been halved by keeping the voltage constant while doubling the number of cores. It is thought that the switching performance of the magnetic core in MPC can be improved as the number of cores increases for the same voltage at the cost of other factors.

Dependence of saturated relative permeability (μ_{rs}) on frequency is described in Figure 5. It can be seen that μ_{rs} is almost independent of frequency for a fixed charge energy because the magnetic core behaves as an air core during the saturated state. Also, it is observed that the permeability of two cores is lower than that of one single core. This is because L_{sat} is constant in the saturated state while the core cross section area has doubled. In fact, μ_{rs} does not indicate the relative permeability of the magnetic core but rather the stray inductance of the core holder divided by the cross section area. Also, it is observed that μ_{rs} does not decrease to 1 due to the stray inductance of the core holder. The stray
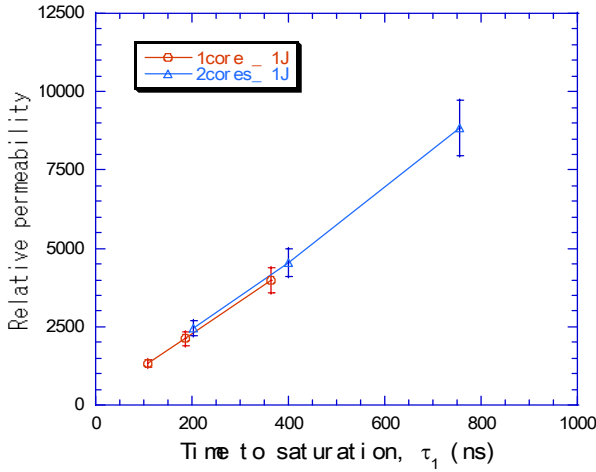
Figure 4. Dependence of unsaturated relative permeability (μ_{ru}) on time to saturation.
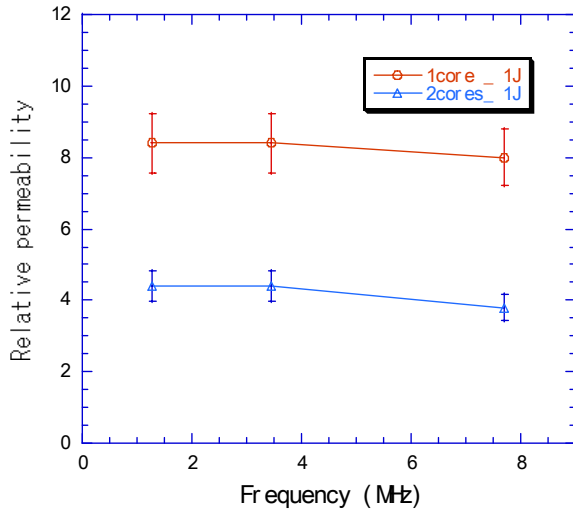

Figure 5. Dependence of saturated relative permeability (μ_{rs}) on frequency.

inductance calculated from the geometry of the core holder can be determined from [7]:

$$L_{holder} = \mu_0 \frac{N^2 \cdot h}{2\pi} \ln\frac{b}{a} \qquad (6)$$

and is about 20 nH where *h, a*, and *b* are the height, the outer radius, and the inner radius of the core holder, respectively.

The saturated inductance calculated from μ_{rs} in Figure 6 using the relation [17]:

$$L_{sat} = \mu_0\mu_{rs}\frac{N^2 \cdot A_e}{l_e} \qquad (7)$$

is also about 20 nH. These same results indicate that the stray inductance of the core holder directly influences the slope of the *B-H* curve in the saturated state and that the inherent μ_{rs} of the magnetic core is nearly unity. From these
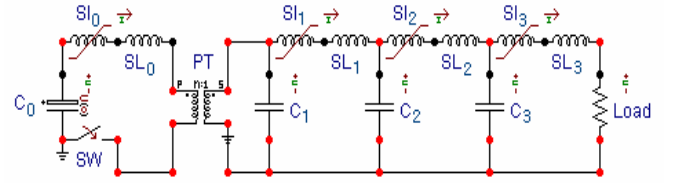

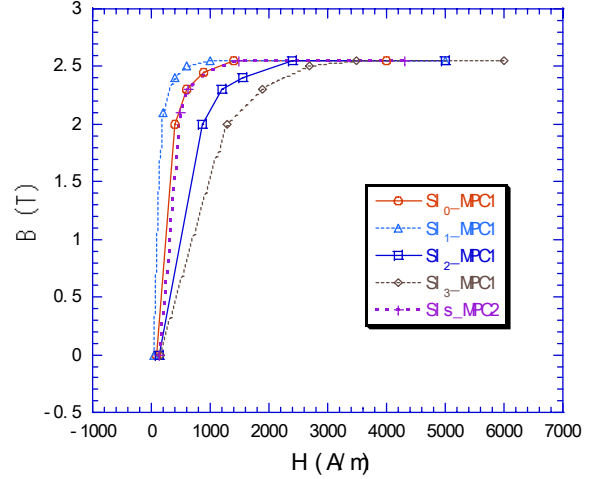**Figure 6.** Schematic diagram of the simulation circuit for a typical 3-stage MPC.

Figure 7. *B-H* curves for the magnetic cores of MPC1 and MPC2.

results, it is evident that the maximum current and effective energy transfer in the saturated state of a real MPC circuit strongly depend on the stray inductances of the circuit.

3.2 EMTP SIMULATION WITH CUSTOM AND IDENTICAL B-H CURVES FOR EACH MPC STAGE

In this study, EMTP [21, 22] has been used to carry out the comparison studies between an MPC (MPC 1 hereafter) with custom *B-H* curves and the other MPC (MPC 2 hereafter) with identical *B-H* curves for each MPC stage. The *B-H* curves of the different permeability characteristics derived in the last section and a *B-H* curve reported by the manufacturer in [2] have been utilized for the magnetic cores of MPC 1 and MPC 2, respectively.

Figure 6 shows the schematic diagram of the EMTP simulation circuit for a typical 3-staged MPC. The simulation circuit has a foremost stage for pulse generation and three subsequent stages for pulse compression, and consists of capacitors (C_0, C_1, C_2 and C_3), saturable inductors (SI_0, SI_1, SI_2 and SI_3), stray inductances (SL_0, SL_1, SL_2 and SL_3), a switch (SW), a pulse transformer (PT) and a matched load. The capacitances of C_0, C_1, C_2 and C_3 are 2.3 μF, 16 nF, 16 nF, and 16 nF, respectively. The charge voltage on C_0 is 2.6 kV. Stray inductances used for each stage are shown in Table 2. These values are based on a real MPC [23]. PT has a function of an ideal step-up transformer with the voltage gain of 12. A 2.3 Ω resistor is used as the matched load.

Table 2. Stray inductances used in the EMTP simulation circuit.

SL$_0$	SL$_1$	SL$_2$	SL$_3$
0.847 µH	0.6 µH	0.276 µH	0.06 µH

Table 3. Calculated Inductances of the magnetic cores of MPC 1.

	SI$_0$	SI$_1$	SI$_2$	SI$_3$
Lu	0.125 mH	15.0 mH	0.143 mH	0.015 mH
Ls	0.024 µH	1.34 µH	0.065 µH	0.011 µH
Lu/Ls	5200	11200	2200	1360

Table 4. Calculated Inductances of the magnetic cores of MPC 2

	SI$_0$	SI$_1$	SI$_2$	SI$_3$
Lu	0.105 mH	5.98 mH	0.292 mH	0.047 mH
Ls	0.024 µH	1.34 µH	0.065 µH	0.011 µH
Lu/Ls	4370	4460	4490	4270

Table 5. Calculated current pulse widths on each stage of MPC 1

	Stage 0	Stage 1	Stage 2	Stage 3
PW (ns)	3140	391	164	75

Figure 7 shows the custom *B-H* curves for SI$_0$, SI$_1$, SI$_2$ and SI$_3$ of MPC 1, and the identical *B-H* curve for SI$_0$, SI$_1$, SI$_2$ and SI$_3$ of MPC 2, respectively. The custom *B-H* curves for SI$_0$, SI$_1$, SI$_2$ and SI$_3$ of MPC 1 were derived from Case 3, Case 6, Case 2 and Case 1 in Table 1, respectively. All the curves show different slopes (that is, μ_{ru}) during the unsaturated state due to the leakage current characteristics of the magnetic core, and same slopes (that is, μ_{rs}) during the saturated state due to the transition of the core from the magnetic material to the air.

Figure 8 shows the flux and current relationships for SI$_0$s, SI$_1$s, SI$_2$s and SI$_3$s of MPC 1 and MPC 2, respectively. The curves were derived from the *B–H* curves shown in Figure 7 using the following relationships:

$$\Phi = N \cdot B \cdot A_e \tag{8}$$

and

$$I = H \cdot l_e / N \tag{9}$$

where Φ is flux [Wb·T], I is current [A]. The numbers of winding turns for SI$_0$, SI$_1$, SI$_2$ and SI$_3$ of MPC 1 and MPC 2 are 3, 16, 4 and 2 respectively, and the numbers of cores for SI$_0$, SI$_1$, SI$_2$ and SI$_3$ are 1, 2, 1 and 1, respectively.

From the derived flux-current curves, it is possible to calculate the unsaturated and the saturated inductances of the magnetic switches. The results are shown in Table 3 and 4. The ratios of the unsaturated to the saturated inductance (Lu/Ls) for SI$_0$, SI$_1$, SI$_2$ and SI$_3$ of MPC 1 are 5300, 11200,
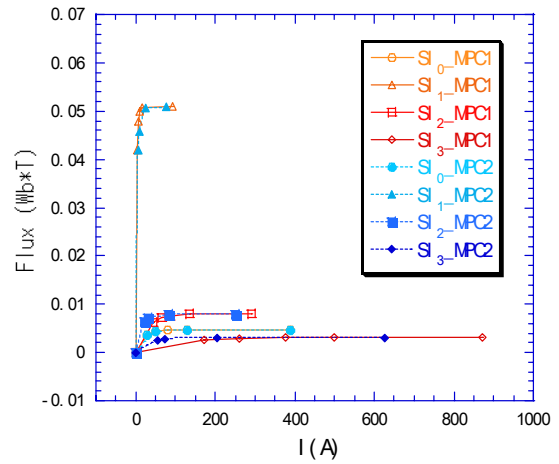
Figure 8. *Φ-I* curves for the magnetic cores of MPC1 and MPC2.

2200 and 1360, respectively, whereas the ratios of the unsaturated to the saturated inductance for SI$_0$, SI$_1$, SI$_2$ and SI$_3$ of MPC 2 are consistently about 4400. It can be expected that the overall performance of MPC 1 decreases as the number of stages increases, whereas that of MPC 2 remains unchanged. Also, it should be noted that this big difference in the ratios plays an important role as a switch in the MPC circuit.

Figure 9 shows the typical voltage and current waveforms on each stage of MPC 1. On switch closure in the pulse generation stage, the magnetic assist by the SI$_0$ follows the switching of the SW for 1.85 µs. Magnetic assist has the effect of reducing the switching loss [4]. Thus, an MPC that consists of the magnetic switch and the solid state switch can be operated with higher repetition rate, longer lifetime and higher reliability than conventional ones.

In Figure 9a, the charge energy in C$_n$ is transferred to C$_{n+1}$ by C-L-C resonance as SI$_n$ saturates with the following relation [23]:

$$\int V(t)dt = \frac{V_{SIn} \cdot \tau_n}{2} \geq N \cdot \Delta B_m \cdot A_e \tag{10}$$

If the leakage current in SI$_n$ is ignored, the voltage $V_n(t)$ on C$_n$ of the n-th stage is given by

$$V_n(t) = V_{n-1} \frac{C_{n-1}}{C_{n-1}+C_n}(1-\cos\omega t) = \frac{V_{n-1}}{2}(1-\cos\omega t) \tag{11}$$

where n = 1, 2 and 3, $\omega = \dfrac{1}{\sqrt{L_T C_T}}$, $L_T = L_{SI_{n-1}} + SL_{n-1}$,

$$C_T = \frac{C_{n-1}C_n}{C_{n-1}+C_n} \ .$$

The voltage waveforms are compressed as the number of stages increases because L$_T$ is designed to decreases with the number of stages in the following way.

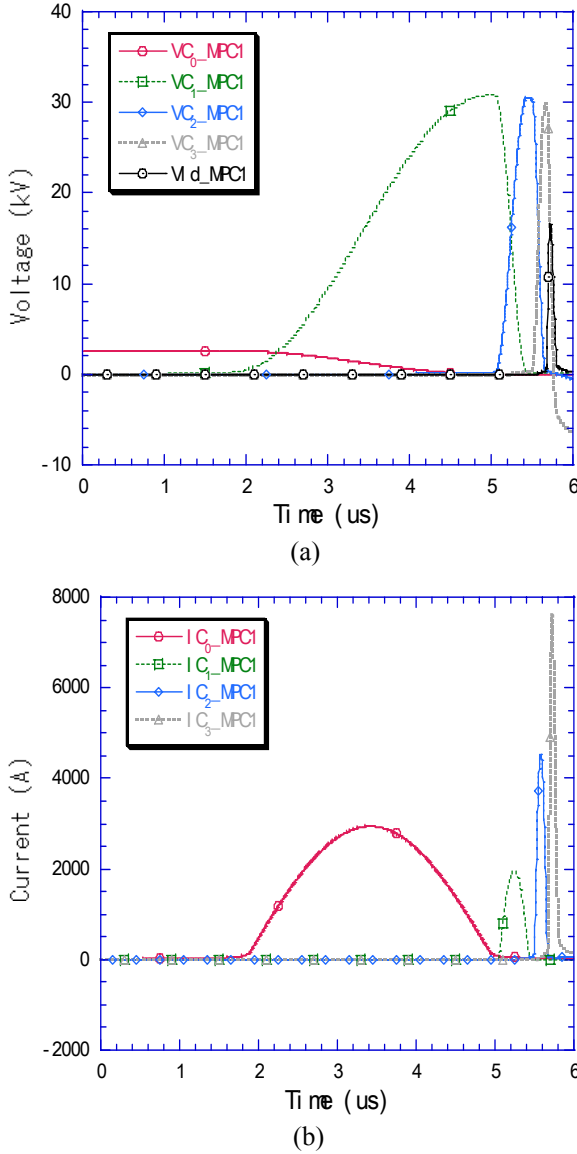V·t for SI$_n$ not to saturate for τ_{n-1} is obtained by

(a)

(b)

Figure 9. Typical voltage (a) and current (b) waveforms on each stage of MPC 1.

$$V \cdot t = \int V(t)dt = \frac{V_{SI_n} \cdot \tau_{n-1}}{2} \tag{12}$$

And, the number of winding turns and the cross sectional area are chosen using the following equation.

$$V \cdot t = N \cdot B_m \cdot A_e \tag{13}$$

Using equation (6), the saturated inductance of the magnetic core is obtained with the determined geometry of the core.

The current pulse width of the n-th stage can be obtained with the values in Table 2 and Table 3 using the following relation:
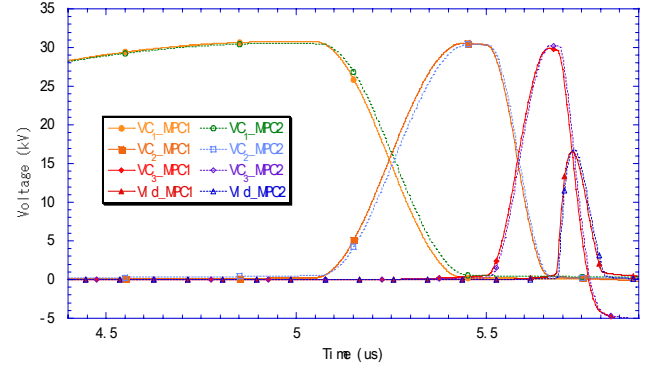
$$\tau_2 = \pi \sqrt{L_T \cdot C_T} \tag{14}$$

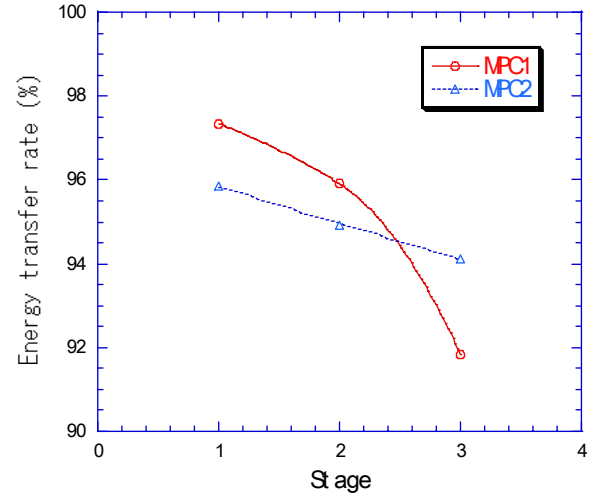**Figure 10.** Comparison of the voltage waveforms between MPC 1 and MPC 2.

Figure 11. Energy transfer rates on each stage.

The calculated current pulse widths on each stage of MPC 1 are shown in Table 5. This results show a good agreement with Figure 9b.

Figure 10 shows the voltage waveforms on each stage of MPC 1 and MPC 2. The charge voltage on C_1 of MPC 2 is lower than that of MPC 1 because SI_1 of MPC 2 has a higher leakage current from Figure 7 than that of MPC 1. Also it is seen that the charge voltage on C_1 of MPC 2 is lagged to that of MPC 2 because equation (10) must be satisfied. The situation is reversed in C_2. The charge voltage on C_2 of MPC 2 becomes higher than that of MPC 1 because SI_2 of MPC 2 has a lower leakage current than that of MPC 1. The phase of voltage waveforms in C_2 remains unchanged because V·t of SI_1 is significantly higher that that of SI_2. The difference of the charge voltages between MPC 1 and MPC 2 becomes larger in the last stage due to the larger leakage current. The energy transfer rate on each stage of the pulse compression part is shown in Figure 11. It should be noted that the transfer rate of MPC 1 decreases exponentially, whereas that of MPC 2 decreases linearly, which indicates that a significant difference can be brought about between custom and identical *B-H* curves for each MPC stage.

4   CONCLUSION

The following critical characteristics for the repetitive pulsed-power operation of MPC have been observed from the derived *B-H* curves for a magnetic core: a high ratio of unsaturated to saturated permeability (μ_{un}/μ_{sat}), a maximum flux swing of about 2.55 T, a high ratio of remanent flux density to saturation magnetic flux density (B_r/B_s) and low core loss.

The unsaturated relative permeability increases with time to saturation and decreasing voltage. The stray inductance of the core holder directly influences the slope of the *B-H* curve in the saturated state.

Comparison studies between MPCs with custom *B-H* curves and identical *B-H* curves for each MPC stage have been carried out using EMTP simulation. The energy transfer rate of the MPC with custom characteristics decreases exponentially, whereas that with identical characteristics decreases linearly.

Based on the present study, it is believed that it is possible to design an MPC with a higher accuracy by using the custom characteristics for the magnetic core of each MPC stage.

ACKNOWLEDGMENT

REFERENCES

[1] Product Bulletin: Pulse Power Core, METGLAS, Allied-Signal Inc., Parsippany, NJ, 1992.

[2] FINEMET, Catalog No. HL-FM9-C, Hitachi Metals, 2005.

[3] T. Sakugawa and H. Akiyama, "An all-solid-state pulsed-power generator using a high-speed gate-turn-off thyristor and a saturable transformer", Electr. Eng. Japan, Vol. 140, No. 4, pp.17-26, 2002 .

[4] W. S. Melville, "The Use of Saturable Inductors as Discharge Devices for Pulse Generators". Proc. IEE 98, pp. 185-207, 1951.

[5] H. Rhinehart, R. Dougal and W. C. Nunnally, "Design and Analysis of a High Power 1kHz Magnetic Modulator", 5th IEEE Pulsed Power Conf., Arlington, VA, pp. 660-663, 1985.

[6] P. W. Smith, *Transient Electronics Pulsed Circuit Technology*, John Wiley & Sons, Ltd., 2002.

[7] M. Hara and H. Akiyama, *High-voltage Pulsed Power Engineering*, Morikita Books, 2002 (In Japanese).

[8] W. Partlo, R. Sandstrom, I. Fomenkov, "A low cost of ownership KrF excimer laser using a novel pulse power and chamber configuration" , Intern. Soc. Optical Eng.-SPIE , Vol. 2440, p.90, 1995.

[9] T. Namihira, S. Tsukamoto, D. Wang, S. Katsuki, R. Hackam, H. Akiyama, Y. Uchida and M. Koike, "Improvement of NOx removal efficiency using short width pulsed power", IEEE Trans. Plasma Sci., Vol. 28, No. 2, pp.434-442, 2000.

[10] Y. Choi, H. Lee, G. Rim, T. Kim, G. Jang, W. Shin and Y. Song, "Analysis of the Pulsed Plasma Reactor Impedance for DeSOx and DeNOx", Jpn. J. Appl. Phys. Vol. 40, pp. 1108-1113, 2001.

[11] Y. S. Mok, Ho W. Lee and Y. J. Hyun, "Flue gas treatment using pulsed corona discharge generated by magnetic pulse compression modulator", J. Electrostatics 53, pp. 195-208, 2001.

[12] Y.-W. Choi, I.-W. Jeong, G.-H. Rim, E. P. Pavlov, C.-S. Choi, H.-K. Chang, M.-H. Woo and S.-P. LEE, "Development of a Magnetic Pulse Compression Modular for Flue Gas Treatment", IEEE Trans. Plasma Sci., Vol. 30, pp. 1632-1636, 2002.

[13] Z. He, J. Liu and W. Cai, "The important role of the hydroxy ion in phenol removal using pulsed corona discharge", J. Electrostatics, Vol. 63, (Is. 4), pp. 371-386, 2005.

[14] E. Njatawidjaja, A. T. Sugiarto, T. Ohshima and M. Sato, "Decoloration of electrostatically atomized organic dye by the pulsed streamer corona discharge", J. Electrostatics, Vol. 63, (Is. 4), pp. 353-359, 2005.

[15] W. Jiang, K. Yatsui, K. Takayama, M. Akemoto, E. Nakamura, N. Shimizu, A. Tokuchi, S. Rukin, V. Tarasenko and A. Panchenko, "Compact Solid-State Switched Pulsed Power and Its Applications", Proc. IEEE, Vol. 92, pp. 1180-1194, 2004.

[16] C. H. Smith and L. Barberi, "Dynamic magnetization of Metallic Glasses", IEEE 5th Pulsed Power Conf., Arlington, VA, pp. 664-667, 1985.

[17] W. C. Nunnally, "Magnetic Switches and Circuits", LA-8862-MS, 1982.

[18] S. Nakajima, S. Arakawa, Y. Yamashita and M. Shiho, "Fe-based nanocrystalline FINEMET cores for induction accelerators", Nuclear Instruments and Methods in Physics Research, Vol. A 331, pp. 318-322, 1993.

[19] J. Choi, T. Yamaguchi, K. Yamamoto, T. Namihira, T. Sakugawa, S. Katsuki and H. Akiyama, "Feasibility Studies of EMTP Simulation for the Design of the Pulsed Power Generator using MPC and BPFN for Water treatments", IEEE Trans. Plasma Sci., Vol. 34, pp.1744-1750, 2006.

[20] K. Masugata, "Analysis of the pulse-compression ratio and the efficiency in the magnetic pulse compression circuit", Trans. IEE Japan, Vol. 117-A, No. 10, pp. 1021-1025, 1997.

[21] Electromagnetic Transient Program (EMTP) Primer, EL-4202 Research Project 2149-1, Final Report, EPRI, 1985.

[22] ATP Rule Book, Argentinian EMTP/ATP User group, 2002.

[23] T. Sakugawa, "Development of a high-repetition-rate pulsed power generator and its applications (paper style)", unpublished.

Jaegu Choi (M'05) was born in Kyoungpook, Korea, on 16 March 1969. He received the B.E. and M.E. degrees in electrical engineering from Kyoung-pook National University in Daegu, Korea in 1994 and 1996, respectively. From 1996 to 2005, he was a senior researcher at Korea Electrotechnology Research Institute (KERI) in Changwon, Korea. And he is currently pursuing the Ph.D. degree at Kumamoto University, Kumamoto, Japan.

Takao Namihira (M'00-SM'05) was born in Shizuoka, Japan, on January 23, 1975. He received the B.S., M.S., and Ph.D. degrees from Kumamoto University, Kumamoto, Japan, in 1997, 1999, and 2003, respectively. Since 1999, he has been a research associate at Kumamoto University. During 2003-2004, he was on sabbatical leave at the Center for Pulsed Power and Power Electronics, Texas Tech University, Lubbock.

Takashi Sakugawa   (M'00) received the M.E. degree from Kyushu University in 1989 and the D.E. degree from Kumamoto University in 2004. He worked at Meidensha Corporation from 1989 to 2004. And he has been an associate professor at Kumamoto University. He is Member of The Laser Society of Japan, The Institute of Electrostatics Japan and JSAP.

Sunao Katsuki (M'99) was born in Kumamoto, Japan, on January 5, 1966. He received the B.S., M.S., and Ph.D. degrees from Kumamoto University, Kumamoto, Japan, in 1989, 1991, and 1998 respectively.
From 1991 to 1998, he was a Research Associate at Kumamoto University, where he is currently an associate professor. During 2001-2002, he was a Senior Researcher at the Plasma and Electronics Research Institute (PERI) of Old Dominion University, Norfolk, VA.

Hidenori Akiyama (M'87–SM'99–F'00) received the Ph.D. degree from Nagoya University, Nagoya, Japan, in 1979. From 1979 to 1985, he was a Research Associate at Nagoya University. In 1985, he joined the faculty at Kumamoto University, Kumamoto, Japan, where he is currently a professor. Prof. Akiyama received the IEEE Major Education Innovation Award in 2000 and the IEEE Peter Haas Award in 2003.